KUTOGLU, A. & HELLNER, E. (1978). *Acta Cryst.* B34, 1617–1623.
LAWS, E. A., STEVENS, R. M. & LIPSCOMB, W. N. (1972). *J. Am. Chem. Soc.* 94, 4461–4467.
MULLEN, D. & HELLNER, E. (1977). *Acta Cryst.* B33, 3816–3822.
PREUSS, H. (1956). *Z. Naturforsch. Teil A*, 11, 823–831.
REES, B. (1976). *Acta Cryst.* A32, 483–488.
SCHERINGER, C. (1977*a*). *Acta Cryst.* A33, 588–592.
SCHERINGER, C. (1977*b*). *Acta Cryst.* A33, 426–429.
SCHERINGER, C. (1977*c*). *Acta Cryst.* A33, 430–433.
SMITH, H. W. & LIPSCOMB, W. N. (1965). PhD Thesis, Havard Univ., Cambridge, Mass., USA.
STEWART, R. F. (1970). *J. Chem. Phys.* 53, 205–213.

Acta Cryst. (1978). A34, 625–634

Electron Microscopy Study of Ordering of Potassium Ions in Cubic $KSbO_3$

BY KATSUMICHI YAGI* AND JOHN M. COWLEY

Physics Department, Arizona State University, Tempe, AZ 85281, USA

(*Received* 2 *November* 1977; *accepted* 2 *February* 1978)

Ordered and disordered states of potassium ions in ⟨111⟩ tunnels in the structure of cubic $KSbO_3$ have been studied by high-resolution electron microscopy. *N*-beam calculations for the images of both the ordered and disordered states reproduce well the observed images. The disordered state changes into the ordered state under electron irradiation during the observations. Electron diffraction from the specimens and optical diffraction from the images show diffuse spots due to small domains of the long-range-ordered state, but no other diffuse scattering due to short-range order has been observed.

1. Introduction

Unlike M^+NbO_3 and M^+TaO_3, $KSbO_3$ does not form the cubic perovskite structure (Goodenough & Kafalas, 1973). It generally has the rhombohedral ilmenite structure. However, by annealing at 1000°C, by applying high pressure at 800°C or by synthesis by a flux evaporation technique at about 1000°C in an open Pt crucible (see, for example, Brower, Minor, Parker, Roth & Waring, 1974), a body-centered cubic structure with a parameter of 9·650 Å is stabilized. The structure is composed of SbO_6 octahedra which share edges or corners with each other forming the network shown in Fig. 1. The figure is seen from the [010] direction, where white octahedra are in the $(x,0,z)$ plane and shaded ones are in the $(x,\frac{1}{2},z)$ plane. The structure is characterized by large tunnels along ⟨111⟩, penetrating each other. They meet at the center of the front face in Fig. 1. The K^+ ions are weakly bound in these tunnels and are mobile along them three-dimensionally. The conductivity behavior has been discussed in comparison with the two-dimensional superionic conductor, β-alumina.

Two structures have been reported for $KSbO_3$. One has space group $Pn3$, where K^+ ions are in an ordered state. The other has $Im3$ with K^+ ions in a disordered state. The positions of the K^+ ions are as follows; along a line in a [111] tunnel from the center of the front face in Fig. 1 to one of the body-centered equivalent positions, the line is surrounded by a sequence of four oxygen triangles denoted by O_1, O_2, O_2 and O_1, where the O_1 triangle has oxygens at the corners of edges shared by neighboring octahedra, and the O_2 triangle consists of atoms at corners of corner-sharing octa-

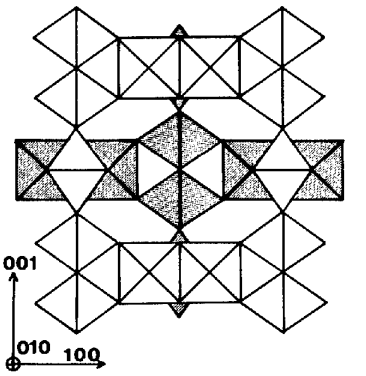

Fig. 1. A [010] projection of the SbO_6 octahedron network in cubic $KSbO_3$. White octahedra, centered on the $(x,0,z)$ plane, form a square arrangement and a large hole. Those shaded are on the $(x,\frac{1}{2},z)$ plane.

* Present address: Physics Department, Tokyo Institute of Technology, Oh-okayama, Meguro-ku, Tokyo 152, Japan.

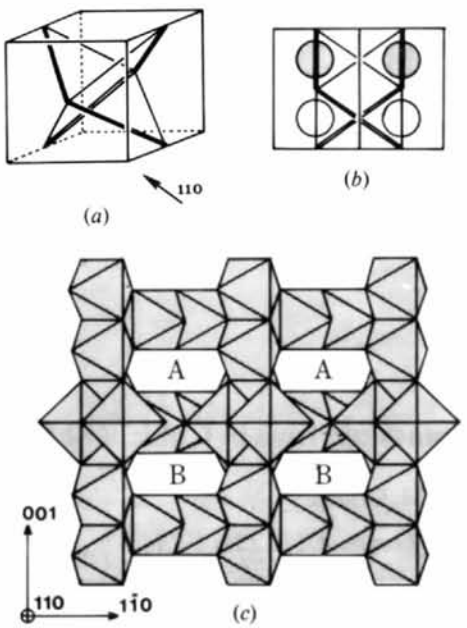

Fig. 2. (*a*) Schematic illustration of the ordered state of K^+ ions along ⟨111⟩ tunnels. Double and single lines represent doubly and singly occupied tunnels respectively. (*b*) [110] projection of the ordered state. (*c*) [110] projection of the SbO_6 octahedron frame. Tunnels *A* and *B* are not equivalent in the ordered state.

hedra. The K^+ ion positions are either octahedral positions formed by O_1–O_2 and O_2–O_1, or O_2–O_2 pairs of triangles. In the ordered state, eight K^+ ions are at O_1–O_2 and O_2–O_1 octahedral positions along the four tetrahedrally oriented ⟨111⟩ directions, and four ions are at O_2–O_2 octahedral positions along the other four ⟨111⟩ directions as shown schematically in Fig. 2(*a*) by double and single ⟨111⟩ lines.

It is readily seen from Fig. 2(*a*) that, if we are concerned with the holes in the projections of the crystal along ⟨100⟩ and ⟨111⟩, there is no difference in the projected potentials for the ordered and disordered states. The difference is seen when we see the crystals along ⟨110⟩, shown by the arrow in Fig. 2(*a*). Fig. 2(*b*) shows schematically the difference. The circles indicate the holes in the crystal along [110] which are seen in Fig. 2(*c*). In (*c*) holes *A* and *B* are equivalent in the disordered state but are not so in the ordered state.

In the present study the technique for high-resolution electron microscopy, recently developed by Iijima (1971) (see also Cowley & Iijima, 1973), was applied to the study of the ordering phenomenon directly in real space. In this technique, images taken under certain electron-optical conditions are directly related to the crystal structure projected along the imaging electron beam with a resolution of about 3·5 Å.

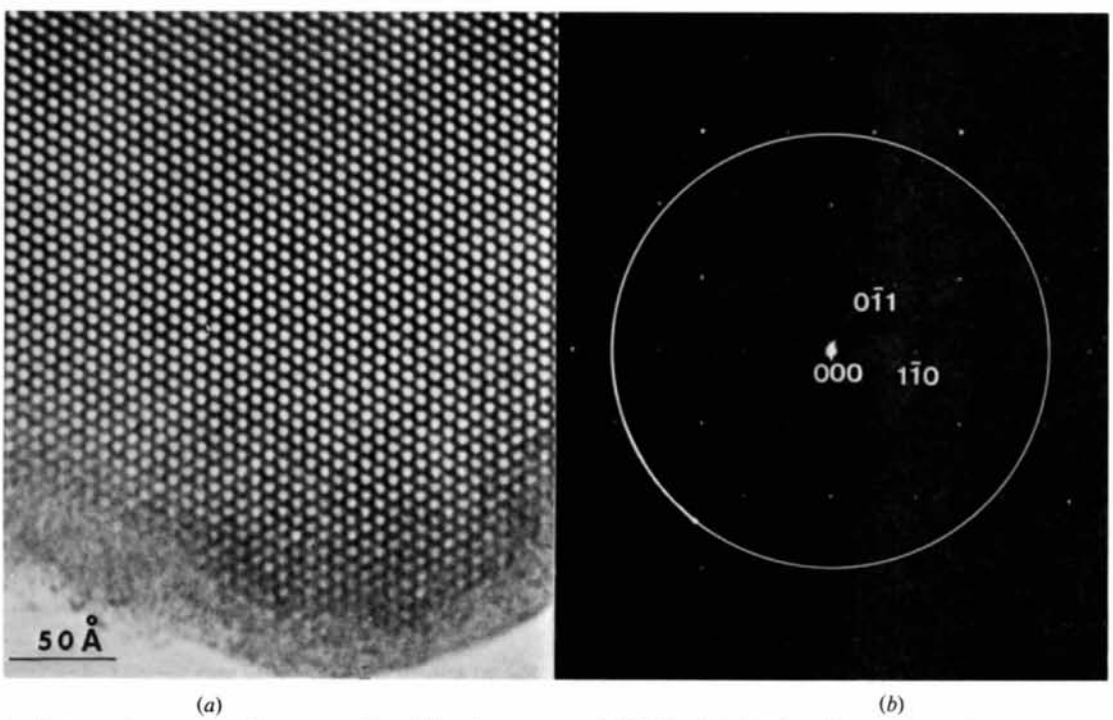

Fig. 3. An electron micrograph and corresponding diffraction pattern of $KSbO_3$ with [111] incidence. The white spots are the ⟨111⟩ tunnels in the structure.

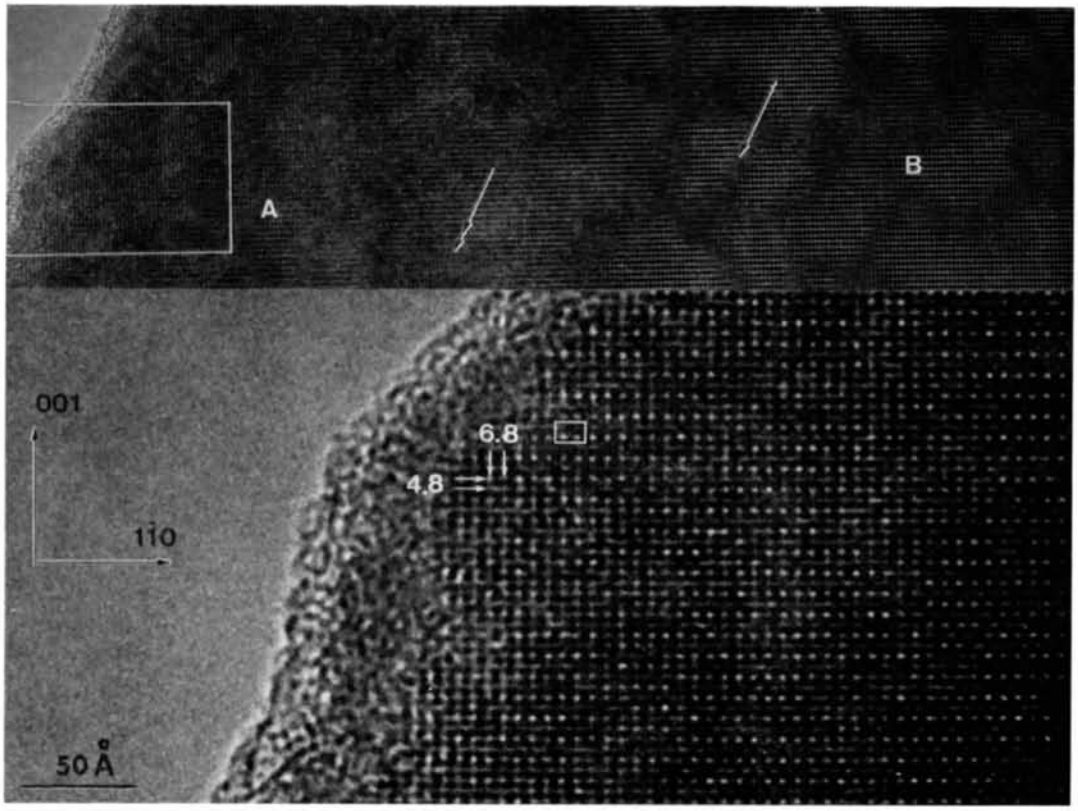

Fig. 4. An electron micrograph of $KSbO_3$ with [110] incidence. The white spots are the [110] tunnels. The ordered state and antiphase domains are seen.

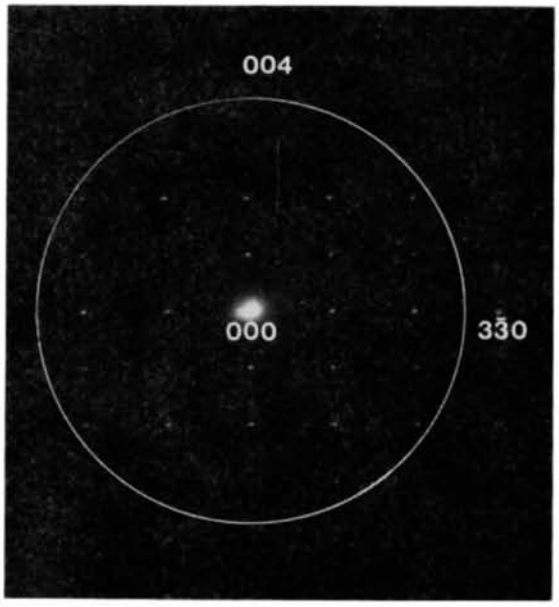

(*c*)

Fig. 4. (*cont.*). (*c*) The corresponding diffraction pattern of $KSbO_3$ with [110] incidence.

2. Experimental

Sample crystals were kindly supplied by Professor M. O'Keeffe of Arizona State University, and were originally synthesized by the flux evaporation technique at the National Bureau of Standards. A JEM 100B electron microscope modified for high-resolution work was used (Iijima, 1971). The sample crystals were ground in an agate mortar and fine fragments were collected on holey carbon films. Very thin crystallites were selected and tilted inside the microscope so that the electron beam was parallel to crystal axes, [110] or [111]. Some parts of the sample crystal were heated in molten $RbNO_3$ or $LiNO_3$ to exchange K^+ ions with Rb^+ or Li^+ ions (heavy and light alkali ions).

3. Experimental observations

Fig. 3 shows an electron micrograph and a corresponding electron diffraction pattern for [111] incidence. A circle in (*b*) shows the objective aperture size. The micrograph was taken at the optimum defocus condition (900 Å underfocus). The hexagonal

arrangement of white spots is nothing but that of ⟨111⟩ tunnels. The image does not show up any contrast due to the order or disorder of K^+ ions in the tunnels.

Fig. 4 shows an electron micrograph and corresponding diffraction pattern of a [110] oriented crystallite. The image was taken under −900 Å defocus condition. The thin area surrounded by white lines in (*a*) is enlarged in (*b*). A cross-grating arrangement of white spots is seen. The spot separations, 4·8 and 6·8 Å in the vertical and horizontal directions, correspond to the (002) and ($\bar{1}$10) lattice spacings. These white spots are the [110] tunnels shown in Fig. 2(*c*). It is noted that some spots are brighter than others and they are in alternate horizontal rows so that the vertical periodicity is doubled. The white rectangle in (*b*) corresponds to Fig. 2(*c*). It will be shown later that the difference of the intensity is due to the ordering of K^+ ions in the ⟨111⟩ tunnels as suggested in Fig. 2(*b*) and (*c*). In relatively thick areas in (*a*), the white-spot arrangement differs from that in thin areas; weaker white spots are at centered positions of brighter spots around mark *A* and an absence of weaker spots around *B*. Irrespective of these fine details of the image contrast, ordered and disordered regions are clearly seen. Antiphase relations between the two ordered domains are also seen. The boundary indicated by a single arrow, for example, is narrow, whereas that indicated by a double arrow is wide. The ordered domains are large in thick areas in (*a*) but they are small in thin areas in (*b*). Fig. 5 shows a through-focus series of images of the same area. It is seen that the images at 0 and −1800 Å defocus do not show the ordered state clearly; black lines indicated by arrows in the correct focus image show the ordered regions weakly. This fact indicates that the optimum defocus condition is necessary not only to obtain the structure image but also to obtain the information about the ordering in $KSbO_3$.

Crystallites initially in the disordered state were found to change into the ordered state. Fig. 6 shows the change; no superlattice spots due to ordering in (1), faint ones in (2) and strong ones in (3). Diffuse scatterings in places other than the superlattice spots are not seen. The corresponding change in the image is shown in Fig. 7. Though the crystallite has changed its orientation slightly from (I) to (VI), the ordering process is clearly seen; in (I) an irregular arrangement of brighter spots is seen. In (II) and (III) brighter spots seem to link in the horizontal directions, forming ordered domains. From (IV) to (VI) the domain size increases and small domains disappear. The arrow indicates the place where a brighter horizontal array changes into a weaker spot array. To find out if there is short-range order in the brighter spots, optical diffraction patterns, shown in Fig. 8, were taken from the

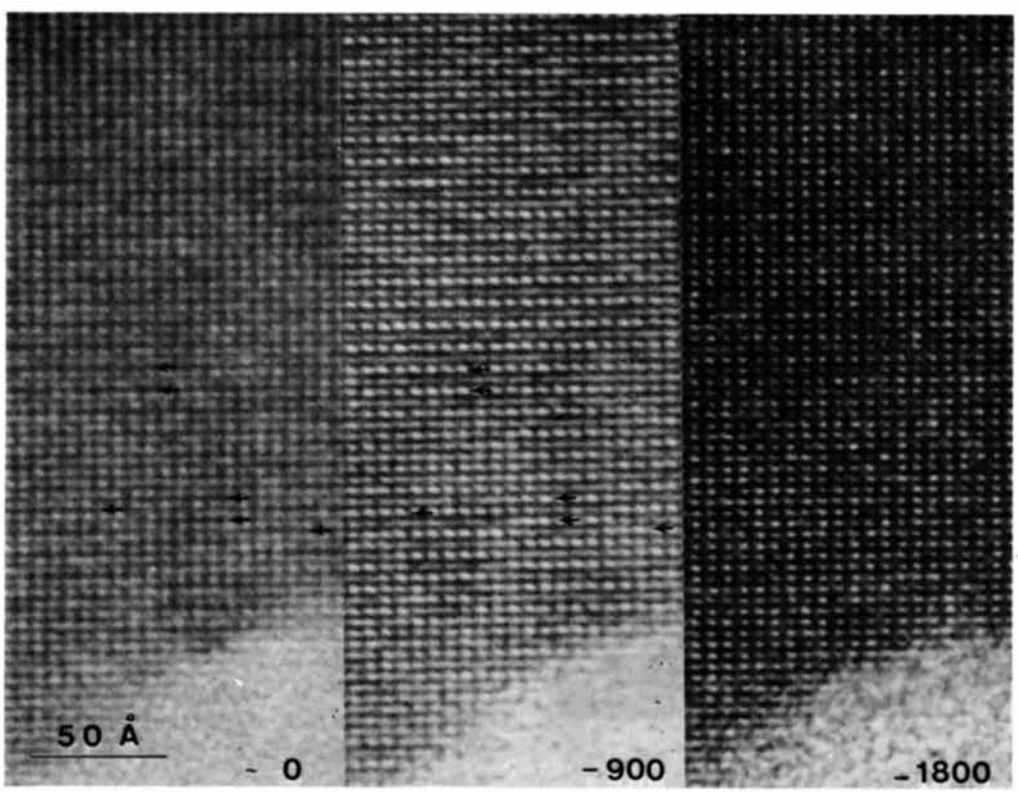

Fig. 5. Through-focus images for [110] incidence.

electron micrographs, especially from thin areas where the domain size is small and brighter spots are irregularly arranged. This is because the diffraction patterns in Fig. 6 are considered to be mainly from a thick part of the crystallite where the ordered regions are very large. However, the patterns show only diffuse spots in the positions of superstructure spots due to the ordering. From (i) to (iv) in Fig. 8 the superstructure spots become sharper and sharper, reflecting the increase of the domain size. The appearance of diffuse spots at superlattice positions in (i) suggests that the crystallite is not in a completely disordered state at stage (i), probably because of the strong irradiation of imaging electrons.

Prolonged irradiation causes the formation of lattice defects and the thin-edge area becomes amorphous.

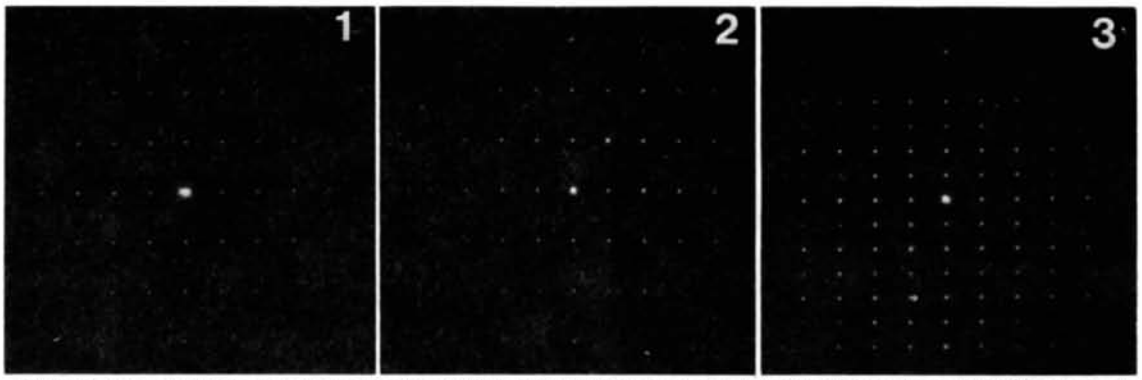

Fig. 6. Diffraction patterns from the same crystallite, which show changes from the disordered (1) to the ordered (3) state while under observation.

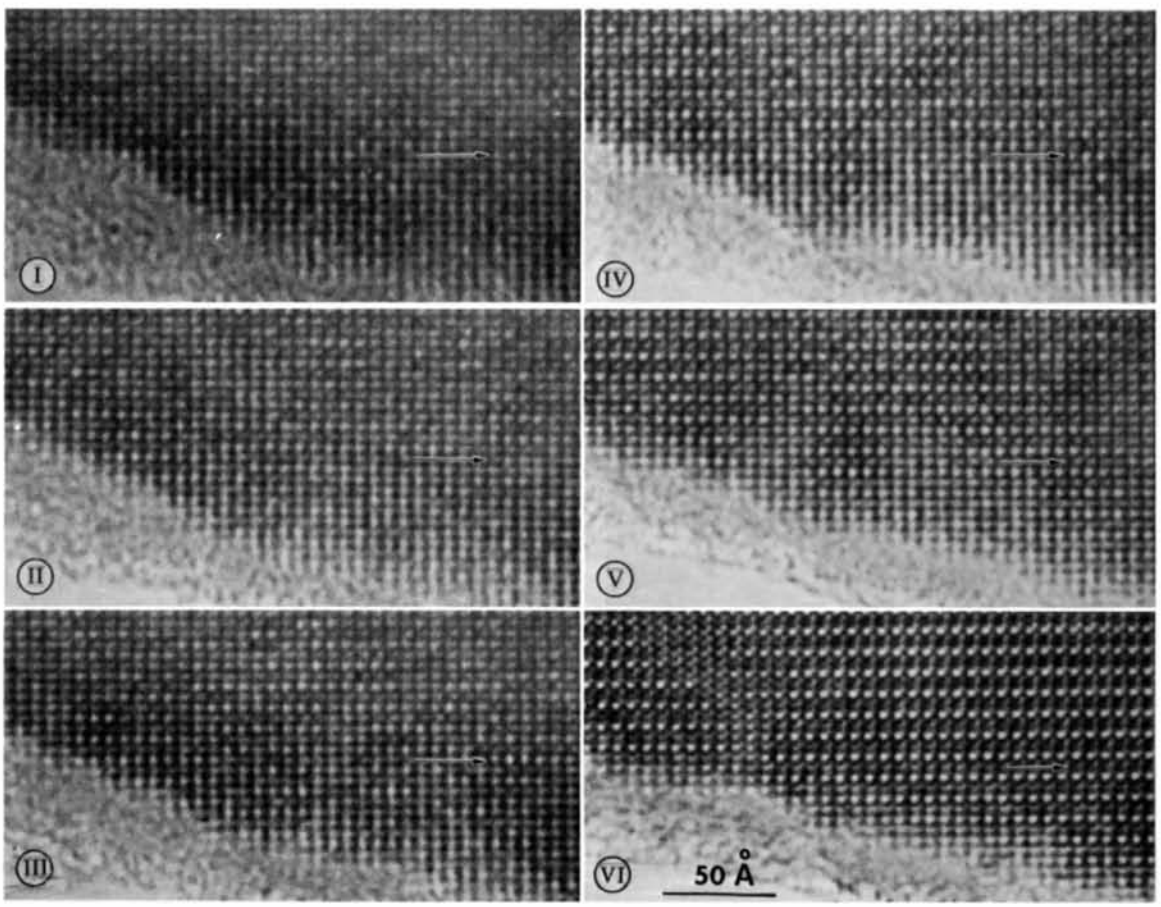

Fig. 7. Successive stages of the ordering process.

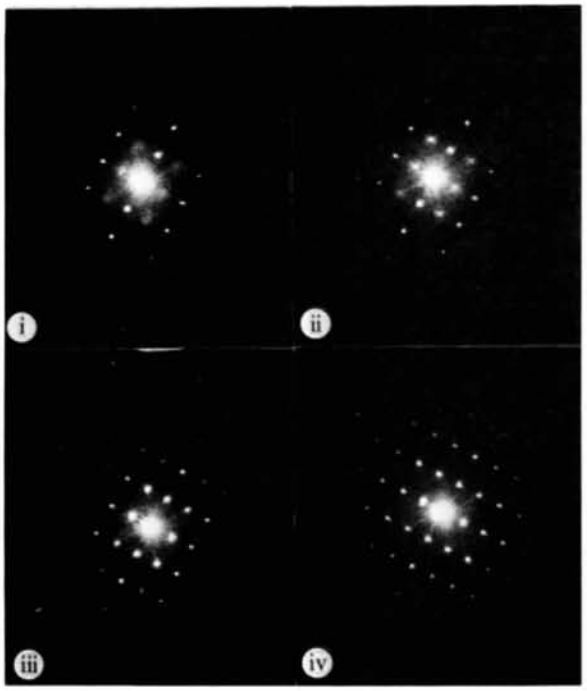

Fig. 8. Optical diffraction patterns from the images of Fig. 7 (I), (II), (IV), (VI). Diffuse scattering due to short-range order is seen at the superlattice positions.

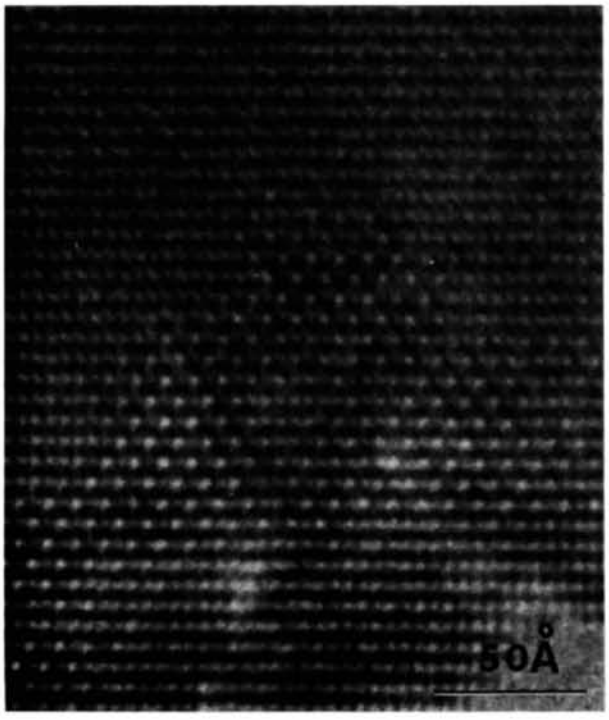

Fig. 9. Electron micrograph after prolonged electron irradiation showing the structural change.

Table 1. *Parameters used in the N-beam calculation of the two-dimensional lattice image*

Accelerating voltage	100 kV
Spherical aberration constant	1·8 mm
Depth of focus	125 Å
Aperture radius	0·35 $Å^{-1}$
Number of beams	
ordered state	193
disordered state	135

Another type of brighter spot arrangement was found to be formed locally, as shown in Fig. 9. The origin of this arrangement has not been determined.

Fig. 10 shows electron micrographs of (*a*) $RbSbO_3$ and (*b*) $LiSbO_3$ crystallites, which were formed from $KSbO_3$ by replacing K^+ ions by Rb^+ and Li^+. As in the case of $KSbO_3$, the ordering of Rb^+ ions is seen. The image does not differ very much from that of $KSbO_3$, though the ordering ions are replaced by the heavier ions. $LiSbO_3$ crystallites did not stand up well under the electron irradiation. The image in (*b*) shows amorphous regions. Though some spots are brighter than the others, it is premature to conclude that the ordering of light Li^+ ions can be seen by high-resolution electron microscopy.

4. Comparison of the observed images with the calculated images

A multislice *N*-beam calculation of the two-dimensional lattice image was done with the program system developed by A. J. Skarnulis and modified by M. A. O'Keefe at Arizona State University. The structures of the ordered and disordered states mentioned in § 1 were assumed. Parameters for the calculations are given in Table 1. The beam-divergence effect was not taken into account. The results for the ordered and disordered states of a [110] crystal 45 Å thick are shown in Fig. 11(*a*) and (*b*). In projected potentials (p.p.), the [110] tunnels are seen, where K^+ ions are located in a different way in the ordered state in (*a*), but not so in the disordered state in (*b*). It is seen that 900 Å underfocus images reproduce the projected potentials and observed images very well: the positions of the [110] tunnels are seen as white spots and the intensities are different in the ordered state but not in the disordered state. It is also noted that the ordered state is not easily recognized in the other defocus images in (*a*) and the difference between (*a*) and (*b*) is small in such images. For the correct-focus image in (*a*), the alternating darker lines are noticed, as is noted in Fig. 5. The intensities of brighter spots in the 1600 Å underfocus image in (*a*) are the same and the ordering can scarcely be noticed, in agreement with the observation in Fig. 5 of the 1800 Å underfocus image. Fig. 12 shows the optimum-focus images for various thicknesses of the

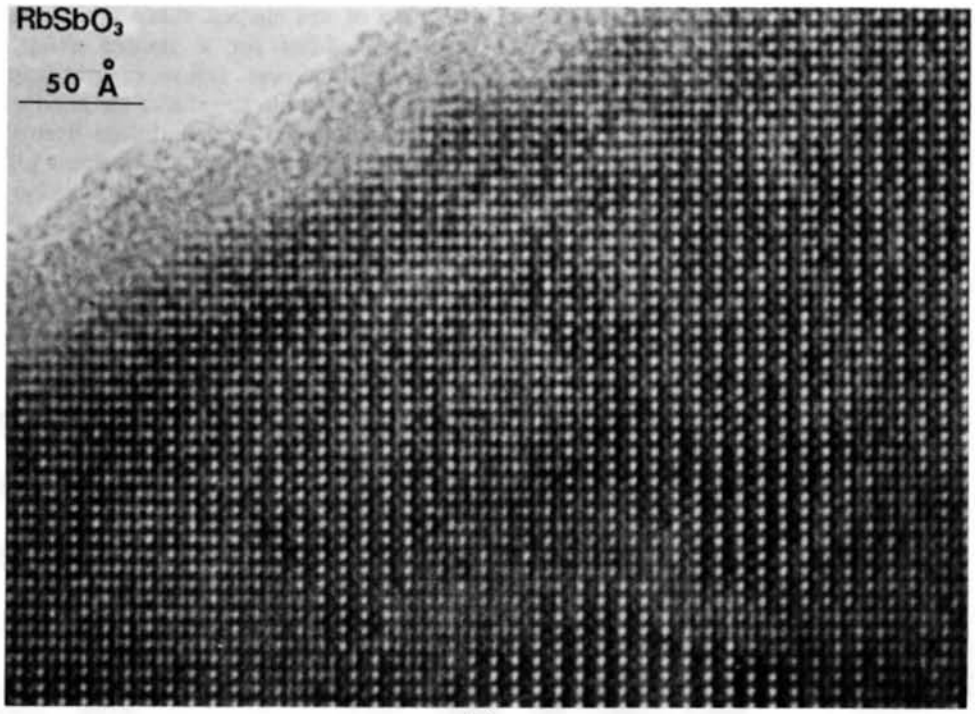

(*a*)

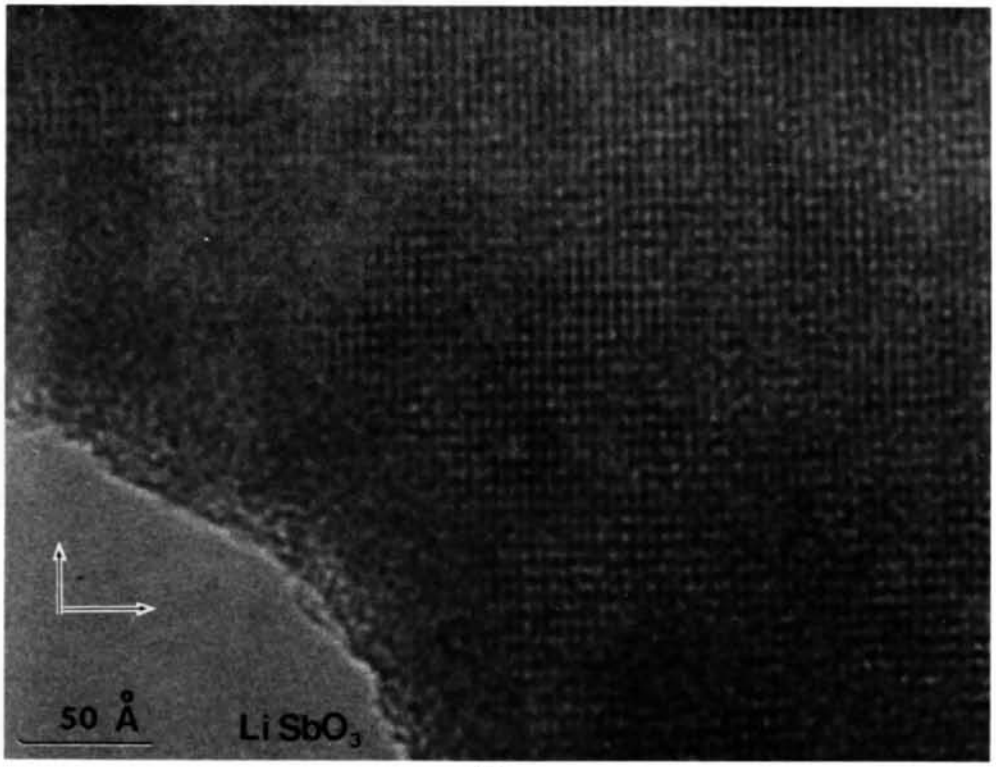

(*b*)

Fig. 10. Electron micrographs of ion-exchanged specimens. (*a*) $RbSbO_3$ and (*b*) $LiSbO_3$.

crystals. In thin regions the difference of white-spot intensities is small and it increases as the thickness increases. For the 90 Å thick image, bright regions are appearing at the centered areas indicated by arrows, and these are actually seen in the area *A* of Fig. 4(*a*). For the 406 Å thick crystal, weaker white spots are absent as in the area *B* of Fig. 4(*a*). These overall agreements indicate that the observed ordered state is actually due to the ordering of K^+ ions.

Between the ordered domains in the micrographs, antiphase domain boundaries are seen. It is not clear from the micrograph whether they are of disordered regions or are slanted sharp boundaries. The images were calculated for a slanted sharp boundary for different thickness ratios of overlapping antiphase domains. Fig. 13 reproduces the results for 45 Å thick crystal. It is seen that the image from the overlapping of equal-thickness antiphase domains (3/3) is similar to the disordered image. This result is also expected from the simple thin-phase object approximation. Slight intensity differences of the two kinds of white spots in the (2/4) ratio show that the formation of the ordered region in $\frac{1}{3}$ of the total thickness (15 Å in this case) is detectable by high-resolution microscopy. So it may be

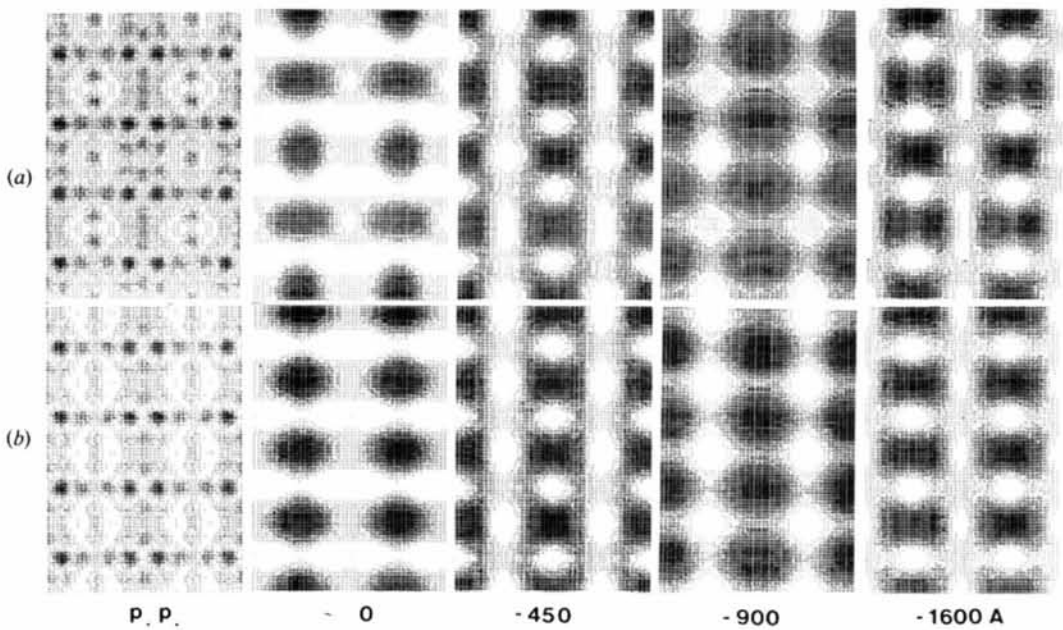

Fig. 11. [110] projected potentials (p.p.) and calculated through-focus images of $KSbO_3$ in the (*a*) ordered and (*b*) disordered states.

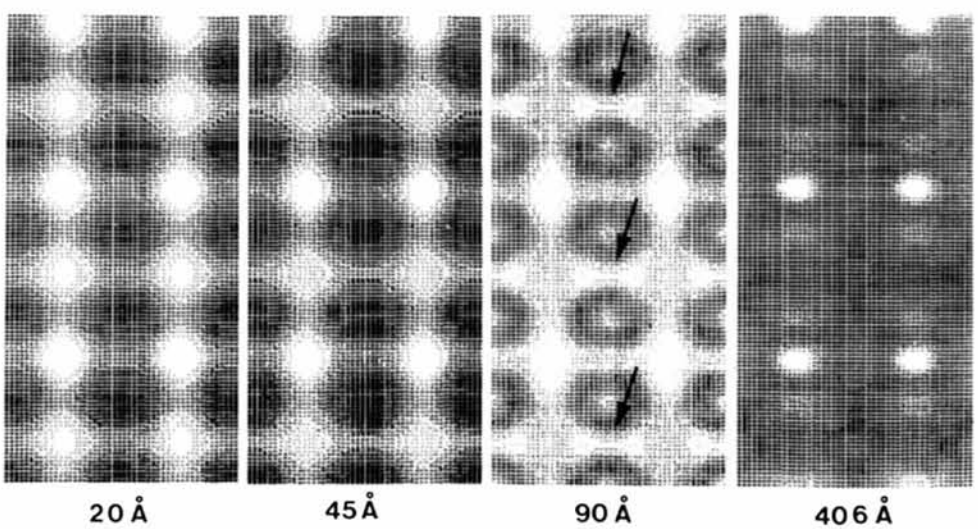

Fig. 12. Optimum-focus images calculated for various crystal thicknesses.

said that narrow boundaries, such as that indicated by the single arrow in Fig. 4(*a*), are slanted sharp boundaries and wide boundaries, such as that indicated by the double arrow, are the disordered state or overlapping areas of equal numbers of small antiphase domains.

5. Summary and discussions

The present study has shown that the ordered images of $KSbO_3$ with [110] incidence are found to be due to the ordering of K^+ ions in the $\langle 111 \rangle$ tunnels, since there is overall agreement between the observed and calculated images. From the experimental point of view, it is interesting to see whether the ordering of light ions, such as Li^+, can be seen by high-resolution electron microscopy. However, sample crystals of $LiSbO_3$ did not stand up well under the electron irradiation.

The observation of diffuse spots in the positions of the superstructure spots in the optical diffraction pattern in Fig. 8 indicates that a crystal of the short-range-ordered state is composed of micro-domains of the long-range-ordered state and there is not a short-range-ordered state which gives rise to diffuse scattering in places other than superstructure spots. The calculated result shown in Fig. 13 indicates that if the thickness of one domain is larger than the thickness of the other domain, having the antiphase relationship, along a [110] tunnel, the tunnel should be seen as a brighter or darker spot. The micrograph in Fig. 7 (I) may be said to represent such a state.

The disordered state may also be considered to be composed of micro-domains, whose sizes, however, are of the order of the unit-cell dimensions. Since along a [110] tunnel there are equal numbers of micro-domains in the antiphase relationship in the disordered state and the [110] tunnel image is not sensitive to the slight deviation from the equal-number configuration, as seen in Fig. 13, the image of the tunnels should be seen with almost equal intensity, as is actually observed.

The ionic conductivity of $KSbO_3$ is very high and the motion of ions is three-dimensional along $\langle 111 \rangle$ tunnels. In the case of β-alumina it is two-dimensional and some sort of ordering or correlation of alkali ions has been reported by X-ray and neutron diffraction studies (Cars, Comés, Deschamps & Thery, 1974; McWhan, Allen, Remeika & Dernier, 1975). It would be interesting to see the correlation directly in real space by high-resolution electron microscopy. However, in contrast to the X-ray and neutron observations, diffuse scattering was not noted in the electron diffraction pattern of Na β-alumina and rapid precipitation of Ag during observation by electron microscope (Roth, 1972) inhibited the high-resolution electron microscope study of correlations of Ag ions in Ag β-alumina.

One of the present authors (KY) expresses many thanks to Dr S. Iijima for his technical advice and discussions on the high-resolution electron microscopy. Thanks are also due to Professor M. O'Keeffe of ASU for his advice and the supply of sample crystals, to Drs A. J. Skarnulis and M. A. O'Keefe for their programs for image calculation and to Dr R. S. Roth for his advice on the ion-exchange experiment. This work was partially supported by the Ministry of Education of Japan and the USA National Science Foundation, Grants GH 36668 and DMR 76-06108.

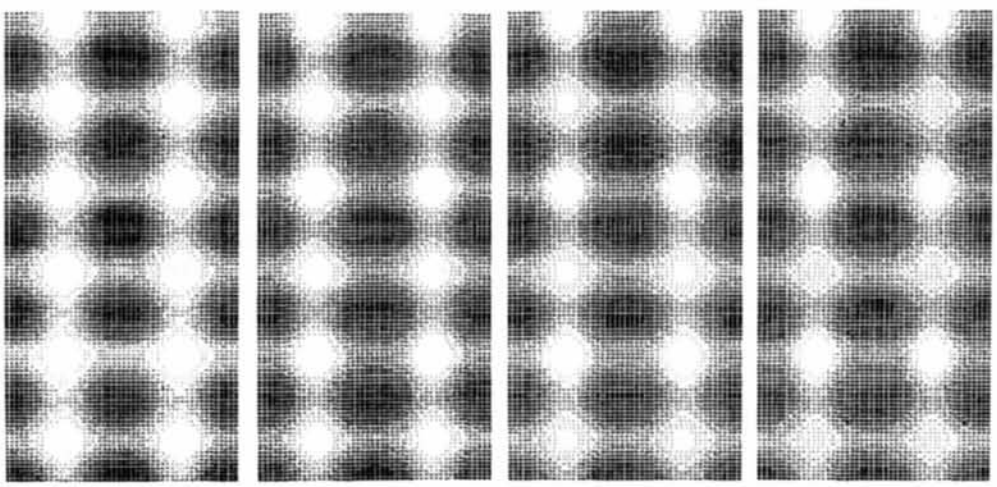

Fig. 13. Optimum-focus calculated images of overlapping antiphase domains with thickness ratio shown in each image.

References

BROWER, W. S., MINOR, D. B., PARKER, H. S., ROTH, R. S. & WARING, J. L. (1974). *Mater. Res. Bull.* **9**, 1045–1052.

CARS, P. Y. L., COMÉS, R., DESCHAMPS, L. & THERY, J. (1974). *Acta Cryst.* A**30**, 305–309.

COWLEY, J. M. & IIJIMA, S. (1973). *Z. Naturforsch. Teil A*, **27**, 445–451.

GOODENOUGH, J. B. & KAFALAS, J. A. (1973). *J. Solid State Chem.* **6**, 493–501.

IIJIMA, S. (1971). *J. Appl. Phys.* **42**, 5891–5893.

MCWHAN, D. B., ALLEN, S. J. JR, REMEIKA, J. R. & DERNIER, P. D. (1975). *Phys. Rev. Lett.* **35**, 953–956.

ROTH, W. L. (1972). *Proc. 5th Mater. Res. Symp. NBS Spec. Publ.* Vol. 364, pp. 129–136.

Short Communications

Contributions intended for publication under this heading should be expressly so marked; they should not exceed about 1000 *words; they should be forwarded in the usual way to the appropriate Co-editor; they will be published as speedily as possible.*

Acta Cryst. (1978). A**34**, 634

On the generation of 'magic integers'.

By J. V. SILVERTON, *Laboratory of Chemistry, National Heart, Lung, and Blood Institute, National Institutes of Health, Bethesda, MD* 20014, *USA*

(*Received* 5 *December* 1977; *accepted* 31 *January* 1978)

The results of a new method of generating 'magic integers' are given. The integers are considerably smaller than those described by Main [*Acta Cryst.* (1977), A**33**, 750–757].

Main (1977) has detailed a method based on the Fibonacci series for generating 'magic integers' for use in the multisolution direct method as described by White & Woolfson (1975). Main's method has the disadvantage that the series are rapidly divergent. In the series with limiting ratio 1·618, the 30th term is 1 346 269 and the 100th approximately $5{\cdot}7315 \times 10^{20}$.

There is, however, another method for generating such integers, obeying Main's rules for efficient sequences, which consists in using a computer to list those series of integers which possess unique sums and differences which themselves are not members of the set. The process is rapid and there appear to be an infinite number of series starting with any given number. The divergence is considerably less than Main's series, for example, the 100th terms of the series starting with 1, 10, 100, 1000 and 1300 are 46 963, 48 493, 48 159, 48 227, and 48 487 respectively. All values less than 80 000 for the series starting with 1 are given in Table 1

Table 1. *The first* 120 *terms of the series of unique integers beginning with unity*

1	3	8	18	30	43	67	90	122	161
202	260	305	388	416	450	555	624	730	750
983	1059	1159	1330	1528	1645	1774	1921	2140	2289
2580	2632	2881	3158	3304	3510	3745	4086	4563	4741
4928	5052	5407	5864	6242	6528	6739	7253	7804	8609
8725	9244	9680	9745	10018	10972	11049	11717	12010	12666
13512	13666	14829	15624	16076	17695	17919	18683	18941	19320
20688	21256	22357	22996	23670	24209	24580	25527	25863	26382
27076	29594	30117	30809	31658	31854	33060	35072	37158	38037
39503	40211	40531	42251	42681	42912	44604	45505	46112	46963
47937	49690	52149	52939	54753	54992	56749	57699	59988	61499
62370	63981	68300	68830	70844	71305	72119	76877	78227	78909

(values for the series mentioned above and also for those starting with 2 through 9 may be obtained from the author).

Monte Carlo tests indicate that the first series leads to r.m.s. deviations comparable with the Fibonacci series of Main but the saving in the number of points needing calculation is large once the number of phases represented exceeds about 14. The results for a representation of 10 phases are given as a typical example. The complementation (Main, 1977) technique for n integers, as adopted in the present work, gives the 'magic integer', $I_i = S_m - S_i$, where S_m is the first member of the series $\geq 2S_n$ and S_i is the ith member of the series. With Main's integers from the Fibonacci series as given, the r.m.s. value of the best fits to the sets of randomly generated phases was 46° with a range of 35° to 56°, in good agreement with the values given by Main (1977). The unique integers in the present work gave an r.m.s. value of 44° with a range of 34° to 55°. It is however debatable whether a linear sampling of the variable is the most efficient since, in a multidimensional closed figure, points tend to lie close to the surface. For example, in a hypersphere of unit radius and dimension 10, 99% of the hypervolume occurs in the shell from 0·631 to 1. Non-linear approaches have not been tried as yet.

References

MAIN, P. (1977). *Acta Cryst.* A**33**, 750–757.

WHITE, P. S. & WOOLFSON, M. M. (1975). *Acta Cryst.* A**31**, 53–56.